***The following resources related to this article are available online at
www.sciencemag.org (this information is current as of July 24, 2008):***

Updated information and services, including high-resolution figures, can be found in the online
version of this article at:
http://www.sciencemag.org/cgi/content/full/311/5760/511

A list of selected additional articles on the Science Web sites **related to this article** can be
found at:
http://www.sciencemag.org/cgi/content/full/311/5760/511#related-content

This article **cites 28 articles**, 11 of which can be accessed for free:
http://www.sciencemag.org/cgi/content/full/311/5760/511#otherarticles

This article has been **cited by** 34 article(s) on the ISI Web of Science.

This article has been **cited by** 15 articles hosted by HighWire Press; see:
http://www.sciencemag.org/cgi/content/full/311/5760/511#otherarticles

This article appears in the following **subject collections**:
Geochemistry, Geophysics
http://www.sciencemag.org/cgi/collection/geochem_phys

Information about obtaining **reprints** of this article or about obtaining **permission to reproduce
this article** in whole or in part can be found at:
http://www.sciencemag.org/about/permissions.dtl

creasing Hg^{2+} concentration. After correcting for the initial shift caused by the new environment, the response of cell-bound DNA-SWNTs fits the model curve created by the same complexes in pure buffer (Fig. 3C). Control experiments produced no additional shift. The successful operation of the complex within living mammalian cells creates opportunities for new molecular probes that operate in the near IR and avoid natural autofluorescence of biological media.

Ion detection is also possible in media that already possess a strong ionic background. A 12,000–molecular weight cut off dialysis capillary was filled with DNA-SWNTs and inserted into whole blood and muscle tissue. The complex was added directly to a black dye solution (optical density > 4). The HgCl$_2$ was still detected through these highly absorptive media (Fig. 3D). The near-IR fluorescence of DNA-SWNTs in the dye solution exhibited the same response as SWNTs in pure buffer. In whole blood and tissue, the presence of interfering absorbers of Hg^{2+} (free DNA, proteins, etc.) predictably shifts the observed sensitivity to larger values (C_0 = 3500 μM in blood; 8000 μM in tissue); however, the DNA-SWNTs still provide a measure of the residual ions that are locally bound to the complex in these heterogeneous media (26).

References and Notes

1. R. Saito, G. Dresselhaus, M. S. Dresselhaus, *Physical Properties of Carbon Nanotubes* (Imperial College Press, London, 1998).
2. A. Hartschuh *et al.*, *ChemPhysChem* **6**, 577 (2005).
3. M. J. O'Connell *et al.*, *Science* **297**, 593 (2002).
4. P. W. Barone, S. Baik, D. A. Heller, M. S. Strano, *Nat. Mater.* **4**, 86 (2005).
5. M. Zheng *et al.*, *Science* **302**, 1545 (2003).
6. F. M. Pohl, T. M. Jovin, *J. Mol. Biol.* **67**, 375 (1972).
7. S. B. Zimmerman, *Annu. Rev. Biochem.* **51**, 395 (1982).
8. T. M. Jovin, D. M. Soumpasis, L. P. McIntosh, *Annu. Rev. Phys. Chem.* **38**, 521 (1987).
9. A. Rich, *J. Biol. Chem.* **271**, 11595 (1996).
10. Materials, methods, and discussions of the modeling are available as supporting material on *Science* Online.
11. J. Duguid, V. A. Bloomfield, J. Benevides, G. J. Thomas, *Biophys. J.* **65**, 1916 (1993).
12. Minor variability in the peak energy in the limit of zero ion concentration (Fig. 1A) is apparently caused by batch-to-batch variation in the DNA-SWNT sample.
13. The change in free energy difference (14) is taken assuming equal propagation lengths as $[\Delta(\Delta G)] = k_B T \ln(C_f/C_{SWNT})$, where C_f and C_{SWNT} are the free and SWNT-bound DNA inflection concentrations, respectively (Fig. 1D). By comparison, the free energy change from the intramolecular contribution alone is 0.1 $k_B T$ per phosphate. The $[\Delta(\Delta G)]$ normally has three contributions arising from hydration, electrostatic, and intermolecular terms.
14. J. L. F. Abascal, J. C. G. Montoro, *Mol. Phys.* **102**, 2141 (2004).
15. F. M. Pohl, *Cold Spring Harb. Symp. Quant. Biol.* **47**, 113 (1982).
16. V. Perebeinos, J. Tersoff, P. Avouris, *Phys. Rev. Lett.* **92**, 257402-1 (2004).
17. M. Rohlfing, *Phys. Rev. B* **62**, 4927 (2000).
18. V. N. Popov, L. Henrard, P. Lambin, *Phys. Rev. B* **72**, 035436 (2005).
19. R. E. Dickerson *et al.*, *Science* **216**, 475 (1982).
20. C. Tung, S. Harvey, *Nucleic Acids Res.* **12**, 3343 (1984).
21. R. Geballe, *Am. J. Phys.* **26**, 287 (1958).
22. A. Wang *et al.*, *Nature* **282**, 680 (1979).
23. The scaling developed by Perebeinos and co-workers (16) has several limitations, including an assumption that the dielectric constant is low and the tube diameters under consideration are greater than 1 nm.
24. S. Rothenburg *et al.*, *Proc. Natl. Acad. Sci. U.S.A.* **102**, 1602 (2005).
25. D. A. Heller, S. Baik, T. E. Eurell, M. S. Strano, *Adv. Mater.* **17**, 2793 (2005).
26. The authors would like to thank S. Denos and M. Gruebele for assistance with circular dichroism experiments, C. Zimmerman and J. Bahr for the donation of rooster blood, and S. McMasters of the School of Chemical Sciences Cell Media Facility for aiding with cell culture and media preparation. This work was supported by NSF grant no. CTS-0330350, DuPont Young Investigator Award 2005, the Defense Advanced Research Projects Agency/ Microsystems Technology Office, and the University of Illinois School of Chemical Sciences.

Rapid Uplift of the Altiplano Revealed Through ^{13}C-^{18}O Bonds in Paleosol Carbonates

Prosenjit Ghosh,[1] Carmala N. Garzione,[2] John M. Eiler[1]

The elevation of Earth's surface is among the most difficult environmental variables to reconstruct from the geological record. Here we describe an approach to paleoaltimetry based on independent and simultaneous determinations of soil temperatures and the oxygen isotope compositions of soil waters, constrained by measurements of abundances of ^{13}C-^{18}O bonds in soil carbonates. We use this approach to show that the Altiplano plateau in the Bolivian Andes rose at an average rate of 1.03 ± 0.12 millimeters per year between ~10.3 and ~6.7 million years ago. This rate is consistent with the removal of dense lower crust and/or lithospheric mantle as the cause of elevation gain.

Earth scientists have attempted to determine the elevation history of Earth's surface by measuring proxies for barometric pressure (1, 2), the thickness of overlying atmosphere (3), the enthalpy of the atmosphere (4), ground temperature (5, 6), and the δ^{18}O value of meteoric water (7–12). Methods aimed at determining atmospheric pressure/ thickness (1–3) are the most theoretically robust but suffer from difficulties in sample availability and interpretation, and as a result have seen little use. The more practical methods, using isotopic data (7–12), have difficulty accounting for climate change or changes in the seasonality of precipitation. Paleobotanical methods of constraining atmospheric enthalpy or temperature (4–6) depend on empirical correlations with plant physiognomy that are of uncertain value when applied to ancient plant communities.

Ghosh *et al.* (13) report the calibration of a new kind of carbonate stable isotope paleothermometer that constrains carbonate growth temperature independently of the δ^{18}O of waters from which they grew. They refer to this method as the "clumped isotope thermometer," because it measures the temperature-dependent clumping of ^{13}C and ^{18}O into bonds with each other in the carbonate mineral lattice. As we show below, this thermometer can (i) constrain the growth temperatures of soil carbonates, which can be compared to a known altitudinal gradient in surface temperature; and (ii) constrain the δ^{18}O of water from which carbonate grew (because both the growth temperature and δ^{18}O of carbonate are known), which can be compared to the altitude dependence of the δ^{18}O of meteoric water; and, by combining these two independent constraints, (iii) constrain the correlation between soil temperature and the δ^{18}O of soil water exhibited by a suite of related samples. This correlation can discriminate between the effects of altitude, climate, latitude, and seasonality in driving changes in temperature and δ^{18}O of water, and thus can help identify records that primarily reflect variations in altitude (rather than other factors) or quantify the contributions of altitude changes to those records.

We determined the stable isotope compositions of pedogenic soil carbonate nodules from paleosols collected in the Bolivian Altiplano [an ~300-km-wide (from east to west), ~1200-km-long (from north to south), 4-km-high plateau perched between the Western and Eastern Cordilleras in the central Andes]. Our

[1]Division of Geological and Planetary Sciences, California Institute of Technology, Pasadena, CA 91125, USA. [2]Department of Earth and Environmental Sciences, University of Rochester, Rochester, NY 14627, USA.

analyses include values of Δ_{47}: a measure of the enrichment of mass-47 isotopologs (principally $^{13}C^{18}O^{16}O$) relative to the randomly expected abundance in CO_2 produced by acid digestion of soil carbonate samples (*13*, *14*). The studied samples (Table 1) come from a sequence of interbedded paleosols, sandstones, and mudstones exposed in the Corque syncline near Callapa (north-central Altiplano; approximately at 17.6°S, 68.2°W). Today, these rocks are at elevations between ~3800 and ~3900 m. Carbonate nodules found in paleosols from this section are generally 0.5 to 3 cm in diameter and are found ~25 to 80 cm below the tops of their host paleosols, and some contain root tubules. These features are consistent with their having grown at depths ranging from centimeters to decimeters around tree or shrub roots. The ages of the paleosols we studied vary between 11.4 and 5.8 million years [as constrained by magnetostratigraphy and $^{40}Ar/^{39}Ar$ dates of volcanic rocks within the section (Table 1) (*15*)].

Values of Δ_{47} for CO_2 extracted from 11.4- to 10.3-million-year-old carbonates average 0.631 per mil (‰) (±0.011‰, $n = 8$ samples), excluding one outlier at 0.546 ± 0.017‰ that we suspect reflects diagenetic resetting (*16*). Carbonates from soils deposited between 7.6 and 7.3 million years ago (Ma) yield CO_2 with Δ_{47} of 0.680‰ (±0.015‰, $n = 2$), and those from soils deposited between 6.7 and 5.8 Ma yield CO_2 with Δ_{47} of 0.706‰ (±0.029‰, $n = 4$) (Table 1 and Fig. 1). The data for the 11.4- to 10.3-million-year-old samples are effectively homogeneous in Δ_{47} within analytical precision, and they probably provide our best in-

dication of the current limits of analytical precision for complex natural samples. These data correspond to carbonate precipitation temperatures of 28.4° ± 2.6°C (SE, ±0.9°C) between 11.4 and 10.3 Ma, of 17.7° ± 3.1°C (SE, ±2.2°C) between 7.6 and 7.3 Ma, and 12.6° ± 5.6°C (SE, ±2.8°C) between 6.7 and 5.8 Ma. Measured paleotemperatures between 11.4 and 10.3 Ma are at the high end of measured modern temperatures at low altitudes (200 to 400 m) on the east flanks of the Andes (*17–19*), suggesting that they grew at a time when the Altiplano had not yet risen to its current altitude and perhaps suggesting warmer temperatures in the Miocene than at present and/or that paleosol carbonates precipitated during the austral summer. Paleotemperatures determined for soils deposited between 6.7 and 5.8 Ma are similar to those currently typical of the warm season (January and February) in La Paz and El Alto, Bolivia [~8° to 10°C, situated at ~4000 m (*17–19*)]. Thus, these data are consistent with the Altiplano having risen to near its modern altitude by 6.7 to 5.8 Ma. Based on the contrast in temperature between the oldest and youngest groups of samples we examined (15.7° ± 2.9°C, 1 SE in the difference between the means) and the vertical gradient in surface temperatures observed in the Andes today [average, 4.66°C/km (*17–19*)], these temperature data alone suggest uplift of 3400 ± 600 m over a period of ~3.6 million years (the span between the end of the 11.4–10.3 Ma period and the start of the 6.7–5.8 Ma period), for an average uplift rate of 0.94 ± 0.17 mm/year. These results are consistent with previous estimates of paleoaltitude for the Altiplano

(Fig. 2). This estimate suffers from potential systematic errors due to changes in latitude and/or climate between the Miocene and the present, and/or due to bias toward an extreme of the seasonal variability in temperature (that is, soil carbonate nodules may not grow evenly throughout the year).

We can also estimate paleoelevations by calculating the $\delta^{18}O$ value of the water from which soil carbonates grew (based on the known growth temperatures and the known carbonate-water oxygen isotope exchange equilibrium) and comparing those results with the known altitudinal gradient in $\delta^{18}O$ of meteoric water (*20*). The $\delta^{18}O_{SMOW}$ (SMOW, standard mean ocean water) values of waters in equilibrium with paleosol carbonates that formed between 11.4 and 10.3 Ma average –8.6 ± 1.1‰ (SE, ±0.4); waters in equilibrium with carbonates formed between 7.6 and 7.3 Ma have average $\delta^{18}O_{SMOW}$ values of –11.8 ± 1.8‰ (SE, ±1.3); and waters in equilibrium with carbonates formed between 6.7 and 5.8 Ma have average $\delta^{18}O_{SMOW}$ values of –14.6 ± 1.2‰ (SE, ±0.6) (Table 1 and Fig. 1). On the basis of the contrast in $\delta^{18}O$ of the parent water between the oldest and youngest groups of samples we examined (6.0 ± 0.7‰, 1 SE in the difference of the means) and the altitudinal gradient in the weighted annual mean $\delta^{18}O$ value of meteoric water observed in the Andes today (*21*), these $\delta^{18}O_{water}$ data suggest that the soils were uplifted 3000 ± 300 m (from 700 ± 200 to 3700 ± 200 m) over ~3.6 million years, for an average uplift rate of 0.83 ± 0.08 mm/year. These results are consistent with our estimate of altitude change based on paleothermometry data alone. However, like that estimate,

Table 1. Stable isotope compositions, growth temperatures, and parental water $\delta^{18}O$ values for Altiplano soil carbonates.

Sample	Age (Ma) (*15*)*	$\delta^{13}C_{PDB}$ of carbonate (*14*)	$\delta^{18}O_{PDB}$ of carbonate (*14*)	Δ_{47} of extracted CO_2 (*14*)	Temperature (°C) (*13*)	$\delta^{18}O_{SMOW}$ of water (*20*)
03BL13	11.42	−9.4	−11.4	0.612 (19)	32.8 (4.6)	−7.5 (0.9)
03BL19	11.32	−6.8	−11.1	0.651 (21)	23.8 (4.6)	−9.0 (0.9)
04BL75	10.88	−9.3	−9.8	0.634 (14)	27.7 (3.2)	−6.9 (0.6)
04BL76	10.74	−8.3	−11.7	0.632 (13)	28.2 (3.0)	−8.7 (0.6)
04BL78	10.58	−9.4	−13.0	0.644 (21)	25.6 (4.7)	−10.5 (0.9)
04BL79	10.53	−8.6	−12.3	0.630 (12)	28.6 (2.8)	−9.0 (0.5)
04BL80	10.46	−10.1	−11.6	0.620 (5)	31.0 (1.2)	−8.2 (0.2)
03BL1	10.33	−8.2	−12.5	0.628 (6)	29.2 (1.4)	−9.3 (0.3)
				11.4 to 10.3 Ma average	**28.4 (0.9)**	**−8.6 (0.4)**
04BL2	7.61	−4.6	−13.9	0.695 (9)	14.6 (1.8)	−13.7 (0.4)
04BL10	7.32	−5.9	−11.5	0.665 (10)	20.8 (2.1)	−10.0 (0.4)
				7.6 to 7.3 Ma average	**17.7 (2.2)**	**−11.8 (1.3)**
04BL21	6.74	−7.7	−14.7	0.681 (4)	17.5 (0.8)	−13.9 (0.2)
04BL24	6.64	−6.7	−13.5	0.713 (12)	11.0 (2.3)	−14.1 (0.5)
04BL25	6.53	−7.0	−14.6	0.750 (8)	4.1 (1.4)	−16.7 (0.3)
04BL30	5.83	−6.5	−14.6	0.679 (13)	18.0 (2.7)	−13.7 (0.6)
				6.7 to 5.8 Ma average	**12.6 (2.8)**	**−14.6 (0.6)**
			Suspected of diagenetic alteration			
04BL69	10.95	−9.9	−8.2	0.546 (17)	50.3 (4.9)	−1.1 (0.8)

*Italic numbers in parentheses at the head of each column refer to references explaining the sources, methods, or algorithms on which the data are based. Analytical uncertainties in $\delta^{13}C$ and $\delta^{18}O$ of carbonate average ±0.02 and ±0.1‰, respectively, and are not shown. Analytical uncertainties in Δ_{47} (numbers in parentheses) are shown for each measurement as the standard error of the mean of all mass spectrometric analyses for a given sample. These are propagated to estimate uncertainties in temperature and $\delta^{18}O$ of water.

this one also suffers from potential systematic errors due to latitude and/or climate change between the Miocene and present, and/or due to bias toward an extreme of the seasonal variability in $\delta^{18}O$ of meteoric water. Moreover, it suffers from potential systematic errors due to evaporative fractionation of oxygen isotopes in soil waters.

The relation between growth temperature and the $\delta^{18}O$ of parental waters recorded by our data for paleosol carbonates (Fig. 1) parallels the relation between mean annual surface temperature and the annual weighted average $\delta^{18}O$ of meteoric water recently measured across the Altiplano and surrounding lowlands, but is slightly offset, on average, from the modern trend toward lower $\delta^{18}O$ at any given temperature and extends to higher temperatures than those observed today in eastern Bolivia. The similarity in slope between our data and the modern mean annual trend shown in Fig. 1 suggests that elevation change is the principal cause of variability in carbonate growth temperature and the $\delta^{18}O$ of soil waters seen in our Miocene record, because other factors (such as changes in global climate or latitude and/or changes in the part of the seasonal cycle sampled by soil carbonates) are predicted to lead to slopes that are different from that of the modern mean annual trend in Fig. 1 (22). This ability to demonstrate the primary role of altitude change in driving variations in temperature and $\delta^{18}O$ of water is a strength of this approach to paleoaltimetry. Still, we must correct for any second-order effects of climate change and latitude change.

Bolivia was 1° to 2° of latitude north of its current position during the mid-Miocene (23), and so its mean annual temperature should have been ~0.3° ± 0.1°C warmer and the $\delta^{18}O$ of its meteoric water 0.9 ± 0.3‰ higher than today (based on modern latitudinal gradients in these variables). Also, low-latitude climate may have been ~1°C warmer in the mid-Miocene (24). Finally, the $\delta^{18}O$ of the ocean was ~1‰ lower in the mid- to late Miocene as compared to today, essentially counterbalancing the change in $\delta^{18}O$ of meteoric water expected from change in latitude (25). Therefore, the modern mean annual trend in Fig. 1 must be shifted to 1.3°C higher temperature at constant $\delta^{18}O$ to equal the expected trend for the mid-Miocene [the similarity in atmospheric circulation patterns from 10 to 15 Ma to the present suggests that there have been no first-order changes in moisture supply (26–28)]. Most important, modern meteoric water $\delta^{18}O$ values and surface temperatures vary seasonally by 10 to 15‰ and several degrees, respectively, across most of the Altiplano and surrounding region. It is possible (perhaps even likely) that soil carbonates grow at different rates in different seasons, and thus might be systematically offset from the mean annual trend toward a seasonal extreme in Fig. 1. Seasonal variations in $\delta^{18}O$ and temperature at any one altitude are correlated with one another, and those correlations are at a high angle to the mean annual trend. Therefore, one can contour lines of constant altitude linking the mean annual trend with the seasonal extreme trends in Fig. 1 (as indicated by the fine dashed lines; only the January/February extreme is shown, for simplicity) and use a sample's position in relation to those contours to estimate its paleoelevation. This approach suggests that the
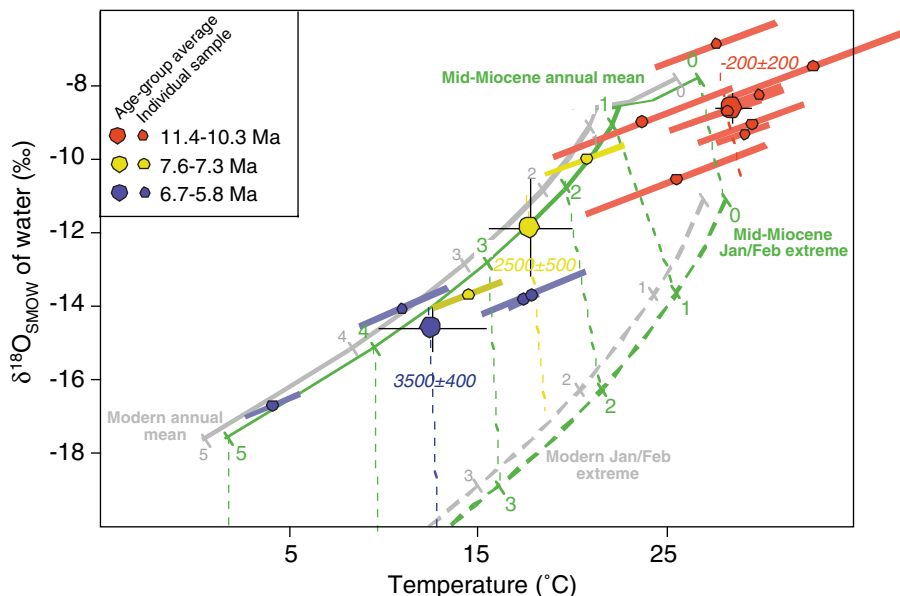
Fig. 1. Plot of the $\delta^{18}O_{SMOW}$ value of water in equilibrium with soil carbonate nodules versus the growth temperatures of those nodules. The small symbols are individual samples from Table 1. The large symbols are averages for the 11.4- to 10.3-Ma, 7.6- to 7.3-Ma, and 6.7- to 5.8-Ma age groups. Error bars for individual measurements are based on external precision in Δ_{47} and $\delta^{18}O$ measurements for acid digestion analyses of carbonates, and they consider the effect of errors in temperature on estimated $\delta^{18}O_{SMOW}$ values of water. Error bars for age groups are ±1 SE of the population. Gray curves show the mean annual trend (solid curve) and trend of January/February (Jan/Feb) extremes (dashed curve) for the relations between surface temperature and the $\delta^{18}O_{SMOW}$ of meteoric water. These curves are contoured for altitude in kilometers. The similar green curves plot the expected location of the mean annual and Jan/Feb extremes in the mid-Miocene, based on inferred changes in the latitude of Bolivia, low-latitude climate change, and secular variation in the $\delta^{18}O$ of seawater. Fine dashed lines connecting the mid-Miocene mean annual trend and Jan/Feb extreme trend show the slopes of seasonal variations in temperature and $\delta^{18}O$ of water at a fixed altitude (we infer that these were the same in the Miocene as today). Paleoaltitudes of age-group averages are estimated by their intersections with this set of altitude contours, as indicated by the red, yellow, and blue dashed lines.

Fig. 2. Constraints on the uplift history of the Altiplano, based on data from this study (colored boxes, with error bars indicating ±1 SE) and paleobotanical constraints (45, 46). Arrows mark the uplift history that is most consistent with both sets of constraints. The average uplift rate between ~10.3 and 6.7 Ma is 1.03 ± 0.12 mm/year, which is approximately three times the rate that could be sustained by crustal shortening driven by plate motions.
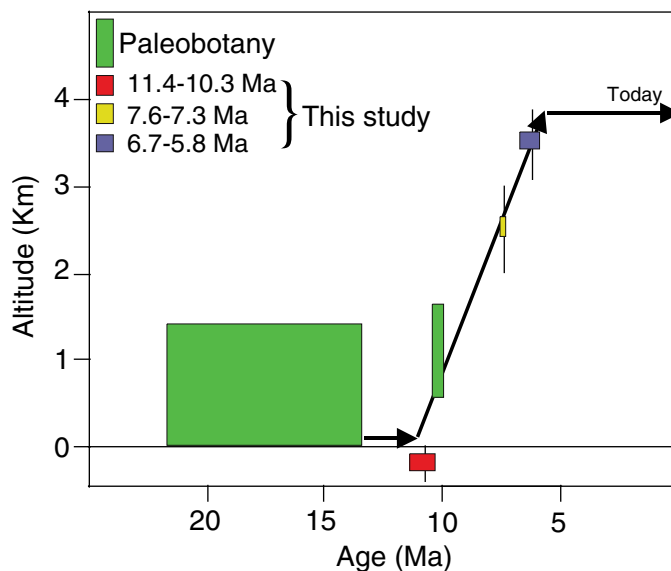
soil carbonates examined in this study preferentially sample warm, low-$\delta^{18}O$ conditions that prevail in the Bolivian austral summer. This is the local rainy season, and may be a time of year when the pedogenic carbonate horizon is most likely to be saturated. Finally, it is possible that evaporation has caused the soil waters from which the carbonates grew to have a higher $^{18}O/^{16}O$ ratio than their meteoric water sources. Based on the magnitude of such effects observed in previous studies of modern soils (29, 30) and the relatively high rainfall received by the northern Altiplano (17–19) (which minimizes evaporative enrichments), we estimate that this effect should be on the order of 0 to 2‰. There is no straightforward way to correct for soil evaporation, but its effects on paleoaltitude estimates using our approach are minimal: If the $\delta^{18}O$ of soil water increased relative to that of meteoric water by 1‰ at a constant temperature, our altitude estimate will be too low by ~200 m at low altitude and by <100 m at high altitude (based on the slopes of isoelevation contours in Fig. 1).

Comparison of our age-group average data (Table 1) with the contours of expected mid-Miocene seasonal variation in temperature and $\delta^{18}O$ of meteoric water (Fig. 1) yields the following paleoaltitude estimates (Fig. 2): –200 ± 200 m between 11.4 and 10.3 Ma, 2500 ± 500 m between 7.6 and 7.3 Ma, and 3500 ± 400 between 6.7 and 5.8 Ma.

The negative altitude obtained by our method for 11.4 to 10.3 Ma indicates a systematic error in our estimate of absolute elevations. Because of the steep slopes of isoelevation contours in Fig. 1, this error is unlikely to result from errors in our estimation of the $\delta^{18}O$ of meteoric water alone. The most likely explanation is that ground temperatures during the mid-Miocene in Bolivia were ~1° to 3°C warmer than expected based on previous estimates of global climate change and South American continental drift. Alternatively, if all soil carbonates underwent small amounts of recrystallization during burial metamorphism, then measured paleotemperatures could be biased upward by several degrees (but no more, because it is not plausible that the 6.7 to 5.8 Ma group grew at temperatures substantially below 10°C). Because of this uncertainty, we suggest that our absolute elevation estimates are likely too low by several hundred meters; assuming that the size of this error does not vary systematically with sample age, it should have an insignificant effect on differences in inferred paleoaltitude between sample age groups.

The elevation history implied by our results and paleobotanical constraints (arrows in Fig. 2) suggests that the Altiplano underwent 3700 ± 400 m of uplift over ~3.6 million years, implying an average uplift rate of 1.03 ± 0.12 mm/year. Visual inspection of Fig. 2 suggests that uplift rate was approximately constant over the sampled period. However, it is possible that rates were higher than this for relatively brief times if elevation change occurred in steps lasting less time than the gaps between each sampled time interval.

The rate of major elevation change of the Altiplano has implications regarding the forces responsible for its uplift. Processes of crustal shortening and isostatic compensation of thickened crust could have led to elevation increases of the Altiplano at rates up to 0.3 mm/year (31). This is approximately one-third the minimum rate of elevation change constrained by our results, seemingly ruling out crustal shortening as a physical cause of the rise of the Altiplano. A mechanism that could explain the rapid uplift of a region the size of the Altiplano is the removal of dense lower crust and/or mantle lithosphere and its replacement by hot, less dense, asthenospheric mantle and an accompanying isostatic rise of the lower density lithospheric section (32–34).

Uplift driven by delamination of the dense lower crust and/or mantle lithosphere could have increased vertical compressive stress beneath the Altiplano plateau, decreased deviatoric compressive stress across the plateau, transformed the Andean fold-thrust belt from a critical to a supercritical state, and increased the forces applied to the lowlands surrounding the plateau (15). We suggest that these changes in the stress field that occurred between ~10 and ~7 Ma in and around the Altiplano contributed to the decrease in the rate of shortening across the Altiplano [independently estimated to have occurred at ~7 Ma (35)], to the eastward propagation of deformation into the sub-Andean zone in late Miocene time [by ~7.6 Ma (36)], and to a late-Miocene decrease in the convergence rate between the Nazca and South American plates (15).

References and Notes

1. D. L. Sahagian, A. A. Proussevitch, W. D. Carlson, *J. Geol.* **110**, 671 (2002).
2. J. C. McElwain, *Geology* **32**, 1017 (2004).
3. J. C. Gosse, F. M. Phillips, *Quat. Sci. Rev.* **20**, 1475 (2001).
4. C. E. Forest, J. A. Wolfe, P. Molnar, K. A. Emanuel, *Geol. Soc. Am. Bull.* **111**, 497 (1999).
5. K. M. Gregory, C. G. Chase, *Geology* **20**, 581 (1992).
6. J. A. Wolfe, *Annu. Rev. Earth Planet. Sci.* **23**, 119 (1995).
7. C. N. Drummond, B. H. Wilkinson, K. C. Lohmann, G. R. Smith, *Palaeogeogr. Palaeoclimatol. Palaeoecol.* **101**, 67 (1993).
8. C. P. Chamberlain, M. A. Poage, D. Craw, R. C. Reynolds, *Chem. Geol.* **155**, 279 (1999).
9. D. L. Dettman, K. C. Lohmann, *Geology* **28**, 243 (2000).
10. C. N. Garzione, J. Quade, P. G. DeCelles, N. B. English, *Earth Planet. Sci. Lett.* **183**, 215 (2000).
11. M. A. Poage, C. P. Chamberlain, *Am. J. Sci.* **301**, 1 (2001).
12. D. B. Rowley, R. T. Pierrehumbert, B. S. Currie, *Earth Planet. Sci. Lett.* **188**, 253 (2001).
13. The Ghosh *et al.* (37) thermometer is based on the abundances in carbonate minerals of carbonate ion groups that contain both a ^{13}C and an ^{18}O atom (that is, $^{13}C^{18}O^{16}O_2^{-2}$). These ionic groups have lower zero-point energies than their isotopically "normal" and singly-substituted relatives ($^{12}C^{16}O_3^{-2}$, $^{13}C^{16}O_3^{-2}$, $^{12}C^{17}O^{16}O_2^{-2}$, and $^{12}C^{18}O^{16}O_2^{-2}$), leading to a thermodynamic driving force that promotes the clumping of rare isotopes into bonds with each other as opposed to being randomly dispersed throughout the mineral lattice. This effect can be described using an isotope exchange reaction among isotopologs of the carbonate ion: $^{12}C^{18}O^{16}O_2^{-2} + ^{13}C^{16}O_3^{-2} = ^{13}C^{18}O^{16}O_2^{-2} + ^{12}C^{16}O_3^{-2}$. The equilibrium constant for this reaction increases with decreasing temperature and can be determined by digesting a carbonate mineral in phosphoric acid and measuring the $\delta^{18}O$, $\delta^{13}C$, and abundance of Δ_{47} isotopologs (mostly $^{13}C^{18}O^{16}O$) in the product CO_2. From these data, one can calculate the enrichment of Δ_{47} isotopologs in product CO_2 relative to the stochastic, or random, distribution of all C and O isotopes among all possible isotopologs. This enrichment, termed the Δ_{47} value, is proportional to the equilibrium constant for the reaction above in reactant carbonate and varies with carbonate growth temperature by the relation $\Delta_{47} = 59,200/T^2 - 0.02$, where Δ_{47} is in units of per mil and T is the temperature in kelvin. Analytical errors in Δ_{47} are on the order of ±0.01 to 0.02, leading to errors in temperature of ~2° to 4°C. The key feature of this thermometer is that it is based on a homogeneous equilibrium within carbonate rather than on a heterogeneous equilibrium between carbonate and water or some other phase. Therefore, unlike conventional carbonate-water oxygen isotope thermometry, it does not require knowledge of the isotopic composition of water from which carbonate grew or of any other phase with which it might have undergone isotopic exchange.
14. Values of $\delta^{18}O$ and $\delta^{13}C$ of soil carbonates were determined using conventional phosphoric acid digestion techniques (38, 39) and were standardized by comparison with similar analyses of the NBS-19 standard distributed by the International Atomic Energy Agency (IAEA). Values of $\delta^{18}O$ measured for carbonates are reported versus the Pee Dee belemnite (PDB) standard, and values of $\delta^{18}O$ calculated for meteoric and soil waters are reported versus the SMOW standard (as indicated by the subscripts on the $\delta^{18}O$ symbol used in the text, table, and figures). Measurements of Δ_{47} were made on these same aliquots of CO_2 generated by phosphoric acid digestion, using instrumentation and methods described in (40) and (13), including changes in sample preparation described in (41). Values of Δ_{47} were calculated based on raw measurements of R45, R46, and R47, using methods described in (41, 42).
15. C. N. Garzione, P. Molnar, J. C. Libarkin, B. MacFadden, *Earth Planet. Sci. Lett.*, **241**, 543 (2006).
16. Sample 04BL69 (depositional age, 10.95 Ma) is significantly lower in Δ_{47} and higher in $\delta^{18}O_{PDB}$ than other samples in the 11.4- to 10.3-Ma age range (Δ_{47} is 0.546 versus 0.612 to 0.651 and $\delta^{18}O$ is –8.2 versus –9.8 to –12.5). These data indicate an equilibration temperature for this nodule of 50°C and a coexisting pore water $\delta^{18}O_{SMOW}$ value of –1.1. These results are consistent with reequilibration of this nodule during burial metamorphism at depths of ~1 to 2 km and are inconsistent with any plausible conditions and water sources for original deposition. We suggest that the portion of this nodule sampled for analysis underwent a cryptic recrystallization event during burial metamorphism and after its original growth near Earth's surface.
17. R. Garreaud, M. Vuille, A. C. Clement, *Palaeogeogr. Palaeoclimatol. Palaeoecol.* **194**, 5 (2003).
18. R. Gonfiantini, M.-A. Roche, J.-C. Olivry, J.-C. Fontes, G. M. Zuppi, *Chem. Geol.* **181**, 147 (2001).
19. Recent meteorological data were taken from a compilation of 8 years of measurements for Bolivian cities found at www.climate-zone.com.
20. The $\delta^{18}O_{SMOW}$ value of water in equilibrium with carbonate was calculated based on the measured $\delta^{18}O_{PDB}$ value of carbonate, the inferred temperature of carbonate equilibration based on the Ghosh *et al.* thermometer (13), and the equilibrium water-calcite oxygen isotope

fractionation determined experimentally by S. T. Kim *et al.* (*43*).

21. The altitude gradients in $\delta^{18}O$ of meteoric water were fit to data for weighted annual mean precipitation and for the minimum monthly average (always in January or February) collected in 1984 and reported in (*18*). These fits used least-squares methods and second-order polynomial equations, and they fit data with r^2 values of 0.98 for both the annual weighted mean and the minimum monthly average. These data were then combined with measured altitude gradients in mean annual temperature and maximum monthly average temperature [also always in January or February (*17–19*)] to yield the relationships between temperature and $\delta^{18}O$ of water plotted as curves in Fig. 1.

22. The slope in Fig. 1 defined by data for carbonate growth conditions and parental waters is 0.34‰/°C. This is indistinguishable from the slope defined by the mean annual altitude gradient in surface temperature and $\delta^{18}O$ of meteoric water in the Altiplano and surrounding area (Fig. 1) (*17–19*) and contrasts with slopes in these dimensions associated with low-latitude climate variations (~0‰/°C for temperatures between 29° and 12°C), latitude variations (~3‰/°C or 0.6‰ per degree of latitude), or seasonality at any one altitude [~ −5‰/°C but varying with altitude; see (*18*) and dashed lines in Fig. 1]. For data documenting these trends, see (*44*).

23. A. G. Smith, A. M. Hurley, J. C. Briden, *Phanerozoic Paleocontinental World Maps* (Cambridge University Press, Cambridge, 1981).

24. S. M. Savin, R. G. Douglas, F. G. Stehli, *Geol. Soc. Am. Bull.* **86**, 1499 (1975).

25. J. Zachos, M. Pagani, L. Sloan, E. Thomas, K. Billups, *Science* **292**, 686 (2001).

26. C. N. Alpers, G. H. Brimhall, *Geol. Soc. Am. Bull.* **100**, 1640 (1988).

27. G. D. Hoke, B. L. Isacks, T. E. Jordan, J. S. Yu, *Geology* **32**, 605 (2004).

28. B. K. Horton, *Tectonics* **18**, 1292 (1999).

29. B. Liu, F. M. Phillips, A. R. Campbell, *Palaeogeogr. Palaeoclimatol. Palaeoecol.* **124**, 233 (1996).

30. T. E. Cerling, J. Quade, in *Continental Indicators of Climate, Proceedings of Chapman Conference, Jackson Hole, Wyoming*, P. Swart *et al.*, Eds. [American Geophysical Union (AGU) Monograph 78, AGU, Washington, DC, 1993], pp. 217–231.

31. Crustal shortening accompanied by isostatic compensation of thickened crust leads to elevation change by the relation $\partial H/\partial T = \partial L/\partial T \times Z/W \times [(\rho_m - \rho_c)/\rho_c]$, where $\partial H/\partial T$ is the rate of elevation gain, $\partial L/\partial T$ is the shortening rate (10 mm/year, based on long-term plate motions), Z is the initial crustal thickness (50 km), W is the width of the deforming region (300 km), ρ_c is the density of the crust (assumed to equal 2.7 g/cc), and ρ_m is the density of the mantle (assumed to equal 3.3 g/cc). See (*15*) for explanations of these choices of values for the physical constants. This relation predicts a maximum rate of elevation gain that is, not considering any elevation losses due to erosion) of 0.3 mm/year.

32. P. Bird, *J. Geophys. Res.* **83**, 4975 (1978).

33. P. C. England, G. Houseman, *J. Geophys. Res.* **94**, 17561 (1989).

34. R. W. Kay, S. Mahlburg-Kay, *Geol. Rundsch.* **80**, 259 (1991).

35. S. Lamb, L. Hoke, *Tectonics* **16**, 623 (1997).

36. L. Echavarria, R. Hernandez, R. Allmendinger, J. Reynolds, *AAPG Bull.* **87**, 965 (2003).

37. P. Ghosh *et al.*, *Geochim. Cosmochim. Acta*, in press.

38. J. M. McCrea, *J. Chem. Phys.* **18**, 849 (1950).

39. P. K. Swart, S. J. Burns, J. J. Leder, *Chem. Geol.* **86**, 89 (1991).

40. J. M. Eiler, E. A. Schauble, *Geochim. Cosmochim. Acta* **68**, 4767 (2004).

41. H. Affeck, J. M. Eiler, *Geochim. Cosmochim. Acta,* in press.

42. Z. Wang, E. A. Schauble, J. M. Eiler, *Geochim. Cosmochim. Acta* **68**, 4779 (2004).

43. S. T. Kim, J. R. O'Neil, *Geochim. Cosmochim. Acta* **61**, 3461 (1997).

44. J. R. Gat, W. G. Mook, H. A. J. Meijer, *Environmental Isotopes in the Hydrological Cycle: Principles and Applications. Volume II: Atmospheric Water* (IAEA, Vienna, Austria, 2001); available at www.iaea.org/programmes/ripc/ih/volumes/volume2.htm.

45. K. M. Gregory-Wodzicki, *Geol. Soc. Am. Bull.* **112**, 1091 (2000).

46. K. M. Gregory-Wodzicki, W. C. McIntosh, K. Velasquez, *Am. Earth Sci.* **11**, 533 (1998).

Freezing as a Path to Build Complex Composites

Sylvain Deville,* Eduardo Saiz, Ravi K. Nalla,† Antoni P. Tomsia

Materials that are strong, ultralightweight, and tough are in demand for a range of applications, requiring architectures and components carefully designed from the micrometer down to the nanometer scale. Nacre, a structure found in many molluscan shells, and bone are frequently used as examples for how nature achieves this through hybrid organic-inorganic composites. Unfortunately, it has proven extremely difficult to transcribe nacre-like clever designs into synthetic materials, partly because their intricate structures need to be replicated at several length scales. We demonstrate how the physics of ice formation can be used to develop sophisticated porous and layered-hybrid materials, including artificial bone, ceramic-metal composites, and porous scaffolds for osseous tissue regeneration with strengths up to four times higher than those of materials currently used for implantation.

Although the potential of layered materials has long been recognized (*1*), their creation requires solving a two-fold problem, namely the design of optimum microstructures and the development of fabrication procedures to implement these designs. Natural materials such as nacre offer a wealth of information to guide such a design process (*2*, *3*). The unique properties of natural layered materials are achieved through fine control of the layer thickness, selection of the right components, and manipulation of roughness and adhesion at the organic-inorganic interface

(*4*, *5*). The ideal fabrication process has to be not only simple but also adaptable enough to fabricate layers with a large number of material combinations and a wide range of layer dimensions. Previous techniques for mimicking nacre are bottom-up chemical approaches (*6*, *7*) that are intrinsically limited to a narrow range of materials exhibiting the proper interfacial reactions and compatibility. Other techniques offer only a coarse control of the layer thickness or have practical limitations regarding the number of layers that can be fabricated (*7*, *8*).

In sea ice, pure hexagonal ice platelets with randomly oriented horizontal *c* crystallographic axes are formed, and the various impurities originally present in sea water (salt, biological organisms, etc.) are expelled from the forming ice and entrapped within channels between the ice crystals (*9*). We apply this natural principle to ceramic particles dispersed in water to

build sophisticated, nacre-like architectures in a simple, two-step approach. Ice-templated (IT), porous, layered materials with layers as thin as 1 μm are first fabricated through a freeze-casting process, which involves the controlled unidirectional freezing of ceramic suspensions. These porous scaffolds are then filled with a selected second phase (organic or inorganic) to fabricate dense composites. By using a natural, self-organizing phenomenon, we allow nature to guide the design and processing.

The physics of water freezing has drawn the attention of scientists for a long time. With few exceptions (*10*), much of this work has concentrated on the freezing of pure water or very dilute suspensions (*9*, *11*). This phenomenon is critical for various applications, such as cryo-preservation of biological cell suspensions (*12*) and the purification of pollutants (*13*). An important observation in these studies is that, during the freezing of such suspensions, there is a critical particle size (*11*) above which the suspended particles will be trapped by the moving water-ice front. Another important observation is that the hexagonal ice crystals exhibit strong anisotropic growth kinetics, varying over about two orders of magnitude with crystallographic orientation. Under steady-state conditions, it is possible to grow ice crystals in the form of platelets with a very high aspect ratio. The ice thus formed will have a lamellar microstructure, with the lamellae thickness depending mainly on the speed of the freezing front. We designed a simple experimental setup (fig. S1) that allowed us to precisely control the freezing kinetics. By freezing concentrated suspensions containing ceramic particles with suitable granulometry, we were

Materials Sciences Division, Lawrence Berkeley National Laboratory, Berkeley, CA 94720, USA.

*Present address: Intel Corporation, 5000 West Chandler Boulevard, Chandler, AZ 85226, USA.

†To whom correspondence should be addressed. E-mail: sdeville@lbl.gov